Micromechanical torque magnetometer with sub-monolayer sensitivity[+]

D. H. Min[a,b], A. McCallum[a], Stephen E. Russek[a], John Moreland[a]

[a] National Institute of Standards and Technology, Boulder, CO 80305

[b] Colorado School of Mines, Golden, CO 80401

Abstract

We have developed a micromechanical torque sensor with sub-monolayer sensitivity for *in situ* monitoring of the magnetic moment of thin films during deposition. The film is deposited onto a microcantilever. The torque on the film is determined by measuring the deflection of the cantilever due to a small ac magnetic field perpendicular to the surface of the film. The microcantilevers have a high mechanical quality factor, large surface area, low spring constant, and high resonance frequency to improve film thickness sensitivity. A phase locked loop is used to minimize the resonance frequency shift of the cantilever due to mass loading and temperature drift that would otherwise affect the magnetic torque measurement. The demonstrated thickness sensitivity for a $Ni_{0.8}Fe_{0.2}$ film and a $Ni_{0.8}Fe_{0.2}$ /Cu multilayer film is less than 0.1 nm.

PACS: 07.55.Jg

Key words: ultra-high vacuum, torque magnetometry, cantilever, fiber optic interferometer

E-mail address: dhmin@boulder.nist.gov.

1. Introduction

This paper describes a new technique for sensing the small magnetic moment changes of ferromagnetic films as each monolayer is deposited. Magnetic film properties are usually determined *ex situ* since it is difficult to implement conventional magnetometer sensors in high vacuum or ultra-high vacuum (UHV) environments. There are several reasons for developing *in situ* magnetometry: (1) It is desirable to measure the magnetic moment of a thin film during the film deposition in order to avoid any degradation of magnetic thin film properties due to possible oxidation after breaking a vacuum. (2) A fundamental understanding of interlayer coupling and interlayer mixing mechanisms can be acheived. (3) Real-time monitoring of thin film magnetic moments during the film deposition becomes a cost-effective possibility.

2. Operating principles

Our approach is based on a micromechanical cantilever sensor customized for thin film magnetometry. The cantilever consists of a rectangular beam "spring" attached to a "paddle" substrate. The film is deposited directly onto the paddle. A small ac field applied perpendicular to the surface of the film causes the spring to vibrate. If the energy stored in the spring cantilever is sufficiently small compared to the anisotropy energy then the deflection of the spring is proportional to the magnetic moment of the film [1]. The dimensions of the micro resonator are shown in Fig. 1(a). The field orientations and torque directions are shown in Fig.1 (b). Fig.1(c) shows the setup for a resonating torque

magnetometer. A pair of SmCo permanent magnets generate the bias field H_0 and a small solenoid generates a perpendicular torque field H_t. The displacement of cantilever can be estimated by for a simple beam bending formula [2]

$$Z = \frac{6T_M l_c^2}{Ew_c t_c^3}$$

where w_c is the cantilever width, E is Young's modulus, l_c is the cantilever length, t_c is the cantilever thickness, and $T_M = \mu_0 V_f M_s H_t$ assuming that the torque on the film acts as a bending moment concentrated at the end of the beam. The V_f is the volume of a film and the M_s is the saturation magnetization of a film. We measured the bias field profile near the center where the paddle (1 mm × 1 mm) is located, and found it to be uniform at 23.8 kA/m in the range ±1 mm from the center. Within the range of ±2 mm from the center, the field was 25.0 kA/m which is a ~5 % change compared to the field at the center. The ac magnetic torque field was H_t = 300 A/m.

The Q value was measured by free decay of the vibration of the beam and found to be 1.050×10^5. The theoretical resonance frequency, f_0, based on a distributed mass model [3] of a silicon paddle cantilever with dimension shown in Fig. 1(a) is 3.783 kHz, which is close to our measured range of 3.956 to 4.020 kHz during a 5 nm deposition of $Ni_{0.8}Fe_{0.2}$. The spring constant is approximately 0.055 N/m based on the cantilever spring dimensions and the modulus of silicon. Given these parameters, the cantilever thermal fluctuations in a 1 Hz bandwidth is

$$Z_{themal} = \sqrt{\frac{2k_B T}{p\, Q K_s f_0}}$$

where $K_s = Ewct_c^3 / l_c^3$ is the spring constant [4]. We therefore predict the ultimate signal-to-noise ratio (SNR) for this setup in the 1 Hz bandwidth of [5]

$$SNR_{thermal} = \frac{Z}{Z_{thermal}} = 6\frac{T_M}{l_c}\sqrt{\frac{p\, Q f_0}{2K_s k_B T}}$$

where Q is the mechanical quality factor, $k_B T$ is the thermal energy, and T_M is the torque due to the magnetic film. Theoretically, we calculate $Z = 2.27 \times 10^{-13}$ m, $Z_{thermal} = 1.13 \times 10^{-16}$ m, and a $SNR_{thermal} = 2.01 \times 10^3$ for a 0.1 nm thick $Ni_{0.8}Fe_{0.2}$ film using the measured saturation magnetization $M_s = 6.8 \times 10^5$ A/m for thin film. We found experimentally that SNR = 1.1 for a 0.1 nm thickness $Ni_{0.8}Fe_{0.2}$ film during the deposition. This is probably due to the vibrational noise of the UHV system. Note that even if vibration could be minimized the instrument would still be limited by the optic fiber interferometer sensitivity $Z_{fiber} = 1.36 \times 10^{-15}\ \mathrm{m}/\sqrt{Hz}$, and $SNR_{fiber} = Z / Z_{fiber} = 166$ for a 0.1 nm $Ni_{0.8}Fe_{0.2}$ film.

3. Experimental setup

A 8 nm thick $Ni_{0.8}Fe_{0.2}$ film is deposited on the opposite side of the grooved surface of the paddle. This is necessary to find the resonance torque frequency of the

cantilever so the magnetometer can be tuned before the deposition. The experimental setup for this specific application is shown in Fig. 2(a). The oscillator chip is mounted in a deposition head (Fig. 2(b)) with the cantilever paddle located between the two SmCo magnets. An optical fiber interferometer (single mode, fiber core: 5 μm), similar to the conventional optical fiber interferometers developed for atomic force microscopy (AFM) [6], is used to measure the cantilever's deflection. A fraction of the laser light (~4 %) passing through a directional coupler is reflected by the fiber facet, and the remainder is reflected by the cantilever paddle surface. These beams interfere with each other and form one reflected beam, which travels back through the fiber and is detected as an output signal by the photodetector. A laser diode is controlled by a diode driver and the wavelength is changed by the laser temperature to be on the steep part of the interference fringe [7]. A phase detector measures the phase difference between the output signal from the interferometer and the signal input to the coil that generates torque field H_t. A proportional-integral-differential (PID) controller and a voltage controlled oscillator (VCO) keep the phase difference the same as the value set in the PID controller. The phase detector, the PID controller, and the VCO make the phase locked loop (PLL) and track the resonance frequency shifts due to the mass loading effect and thermal drift during the film deposition. The instrument therefore provides a signal proportional to the magnetic signal separate from mass loading and thermal drift effects.

4. Oscillator chip fabrication

At the heart of this magnetometer design is a silicon oscillator chip fabricated from a double-sided polished <100>-oriented single-crystal silicon wafer of which the diameter and thickness are 75 mm and 350 μm respectively. Fig. 3 shows the diagram of the oscillator chip assembly which consists of two parts. One is a cantilever paddle (Fig. 3(a)) and the other is a deposition mask (Fig. 3(b)) that is used to ensure that the film deposits only on the paddle. If the magnetic film is deposited onto the cantilever, the signal would not be proportional to the magnetic moment of the deposited film due to the reduction in Q [8]. The deposition mask has a square hole slightly larger than the paddle dimensions. The surface of the paddle is grooved (width 5 μm, depth 4 μm, period 50 μm) to minimize the eddy current effect that possibly reduces the output signal slightly [9]. These two parts are bonded together as shown in Fig. 3(c). Details of the chip fabrication process are shown in Fig. 4(a). First, we start with a buffered oxide etch (BOE) to remove the oxide from the silicon wafer. Then, we make grooves in the cantilever paddle using several steps of lithography and deep reactive ion etching (DRIE). A cantilever thickness of 40 μm is determined by timing the DRIE process. Second, we deposit 0.4 μm Si_3N_4 on both sides of the wafer and the backside nitride is then patterned using reactive ion etching (RIE). The cantilever release process is based on a KOH anisotropic etch (30% by weight with 2-3 % of isopropyl alcohol (IPA), and an oxygen bubbler at 75°C) through a silicon wafer with a lithographically patterned Si_3Ni_4 layer as a wet etch mask in the KOH solution. After the KOH etch, the Si_3Ni_4 layer on the front side is removed before magnetic film deposition. The roughness of the paddle surface is

important because it will influence the magnetic properties of the deposited film. In particular, the anisotropy of the film can be strongly related to the substrate roughness. Fig. 5 shows atomic force microscope (AFM) images of the paddle surface before and after the 5 nm $Ni_{0.8}Fe_{0.2}$ film deposition. The rms surface roughness is R_{rms} = 0.89 nm for the paddle before the film deposition and R_{rms} = 1.11 nm after the film deposition compared to the surface roughness of R_{rms} = 0.26 nm of unprocessed Si and of R_{rms} = 0.31 nm for $Ni_{0.8}Fe_{0.2}$ 5 nm deposited on unprocessed Si. According to the AFM images of the $Ni_{0.8}Fe_{0.2}$ on the paddle, after nitride processing, we find that the substrate tilt considering long range surface roughness over a few micrometers is less than 3º. This is probably not a major source of anisotropy and can be neglected. The short range roughness of the $Ni_{0.8}Fe_{0.2}$ film after nitride processing, however, is not negligible compared to similar films on the unprocessed wafers. We are carefully developing fabrication steps to improve cantilever roughness in order to address this issue.

Once the nitride has been removed, 5 μm of SU8 [10] photoresist are spun onto only the silicon frame surrounding the cantilever paddle. The SU8 acts as a spacer to fix the distance between the fiber end and the paddle surface in the final assembly. The cantilever frame is connected to the rest of the wafer by break-off tabs in order to eliminate the need for wafer dicing, shown in Fig. 3(a). The finished cantilever is shown in Fig. 4(b).

Once the oscillator chips are fabricated, they are mounted in the deposition head as shown in Fig. 2(b). The cleaved end of the optical fiber is set above the cantilever at a distance that is determined by the thickness of the SU8 photoresist. The detailed process for SU8 can be found in Ref. [11].

5. Thin film deposition measurements

Magnetron sputter gun deposition sources were used to deposit $Ni_{0.8}Fe_{0.2}$, $Ni_{0.8}Fe_{0.2}$/Cu multilayer films onto the cantilever paddle. Depositions were done in an ultra-high vacuum chamber with a base pressure of 2.6×10^{-6} Pa that is routinely obtained after a 100 °C bake-out for 12 h. During the deposition, the background pressure was 1×10^{-5} Pa of Argon. The magnetic moments of $Ni_{0.8}Fe_{0.2}$ and $Ni_{0.8}Fe_{0.2}$/Cu multilayer films were measured as a function of film thickness during the deposition. The film thickness was determined with a commercial quartz crystal thickness monitor within an accuracy of 0.1 nm. The films were deposited with a deposition rate ranging from 0.17 to 0.18 nm/s for $Ni_{0.8}Fe_{0.2}$ and ~0.088 nm/s for Cu film. Fig. 6(a) shows the graph of the output signal vs. thickness for $Ni_{0.8}Fe_{0.2}$ (5 nm) deposition. As shown in the graph, the magnetic signal does not increase up to film thicknesses around 1.4 nm, indicating that magnetically dead layers are created at the very beginning stage of deposition. These layers are probably due to the nucleation stage of the film growth and the formation of silicide at the interface between the Si substrate and the metallic film. For film thicknesses greater than 1.4 nm, the magnetic signal increases with $Ni_{0.8}Fe_{0.2}$ thickness. The monitoring result of $Ni_{0.8}Fe_{0.2}$/Cu multilayer is shown in Fig. 6(b). The magnetically dead layers were also found at the beginning of the film growth of the first layer of $Ni_{0.8}Fe_{0.2}$. The magnetic signal increases with $Ni_{0.8}Fe_{0.2}$ deposition after ~1 nm and the signal stays constant during the Cu deposition before increasing again with another $Ni_{0.8}Fe_{0.2}$ deposition. We believe that the magnetic signal at the interface between Cu and

$Ni_{0.8}Fe_{0.2}$ does not correspond to a sharp transition because there is some intermixing between the Cu and $Ni_{0.8}Fe_{0.2}$. We estimate the thickness of the first and second intermixing regions to be about 0.5 nm and 0.9 nm respectively based on the data in Fig. (6b).

In summary, we have developed an instrument for monitoring the magnetic moment of thin films and multilayers, with submonolayer sensitivity during the film deposition. This instrument combines custom micromachined mechanical torque sensors with an interferometer similar to that developed for atomic force microscopy to achieve unprecedented magnetic thickness sensitivity at room temperature. Our results show that this instrument has promise for the study of magnetic interlayer coupling mechanisms such as RKKY and superexchange of thin magnetic films [12-14].

Figure captions

Figure 1. A micromechanical torque magnetometer: (a) Dimensions of cantilever spring and paddle. (b) Torque direction due to a saturation magnetization M_s crossed into the ac torque field H_t. (c) Setup diagram of cantilever operation.

Figure 2. Schematic diagram of experimental setup: (a) components of a resonating torque magnetometer. (b) Cross-sectional diagram of deposition head: where A: fiber core (5 μm diameter), B: clad, C: oscillator chip, D: ceramic material, E: screw, F: fiber optic part, G: SmCo permanent magnet, H: SU8 photoresist, I: SmCo magnet, I: Cu support for SmCo magnet, J: coil, K: deposition shield, L: deposition hole.

Figure 3. Schematic diagram of oscillator chip: (a) cantilever paddle and its cross section, (b) deposition mask and its cross section, (c) the cross-sectional view of oscillator chip assembly.

Figure 4. Diagram of cantilever paddle process steps: (a) the fabrication process steps of the cantilever paddle with SU8 spacer, (b) the photograph of finished paddle cantilever.

Figure 5. AFM images of (a) unprocessed bare Si surface, (b) surface of 5 nm NiFe film on the bare Si surface, (c) paddle surface after the nitride film is removed by RIE, and (d) surface of 5 nm NiFe film on the paddle.

Figure 6. Magnetometer response as a function of film thickness measured with a quartz crystal micro-balance (QCMB) for $Ni_{0.8}Fe_{0.2}$ (5 nm) and $Ni_{0.8}Fe_{0.2}$ (3 nm)/Cu (3 nm) multilayer films.

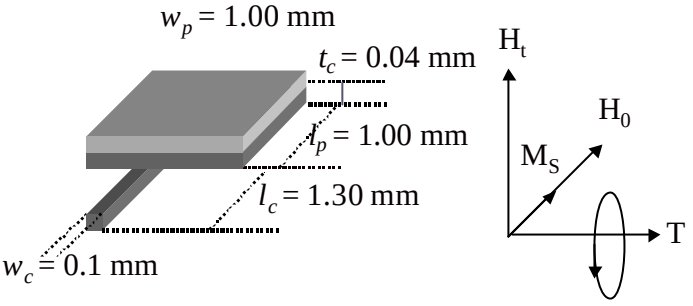
w_p = 1.00 mm
t_c = 0.04 mm
l_p = 1.00 mm
l_c = 1.30 mm
w_c = 0.1 mm
H$_t$
H$_0$
M$_S$
T

(a) (b)

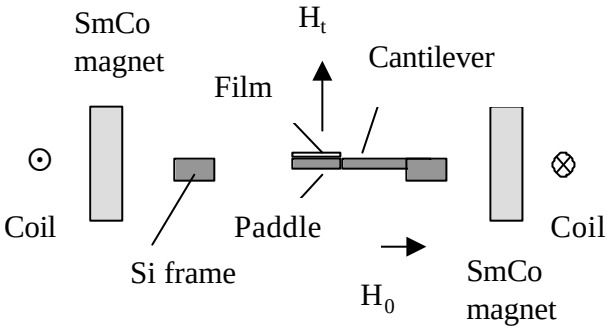
SmCo
magnet
H$_t$
Cantilever
Film
Coil
Paddle
Coil
Si frame
H$_0$
SmCo
magnet

(c)

Figure 1

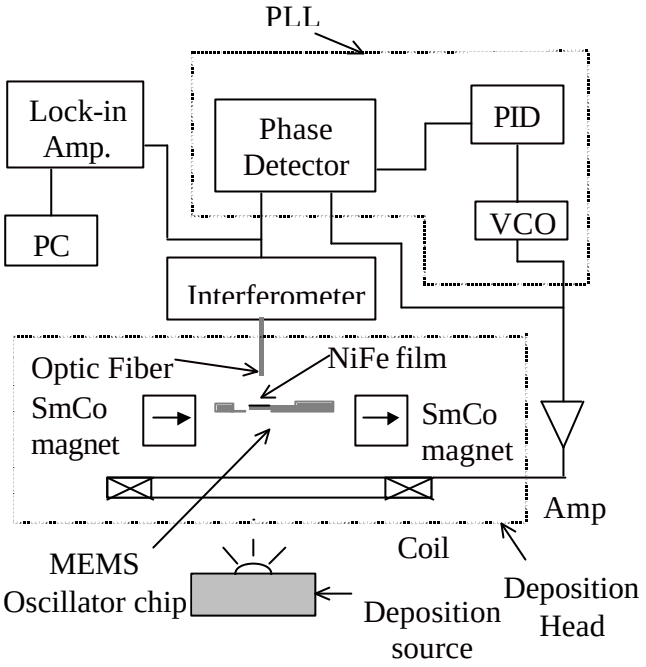
PLL
Lock-in Amp.
Phase Detector
PID
VCO
PC
Interferometer
Optic Fiber
NiFe film
SmCo magnet
SmCo magnet
Amp
MEMS Oscillator chip
Coil
Deposition source
Deposition Head

(a)

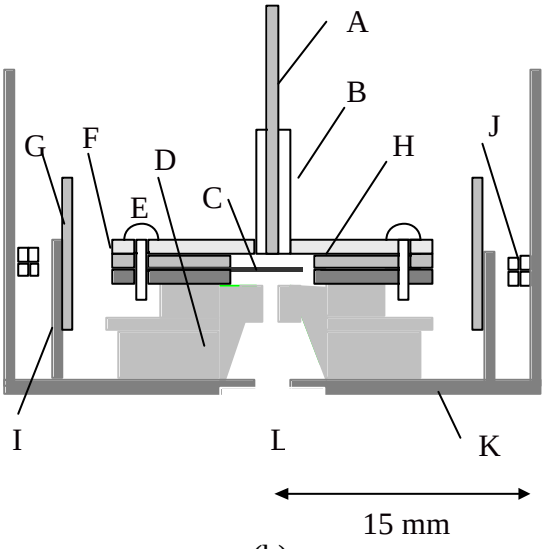
A
B
G
F
D
H
J
E
C
I
L
K
15 mm

(b)

Figure 2

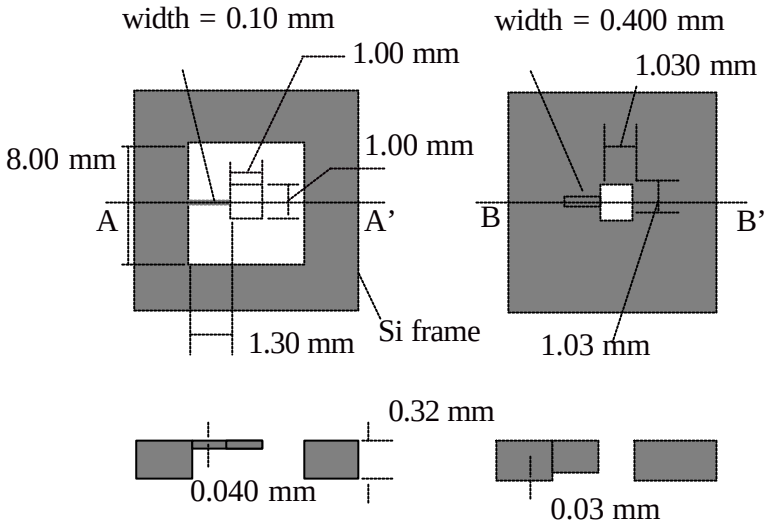
width = 0.10 mm
1.00 mm
8.00 mm
1.00 mm
A
A'
1.30 mm
Si frame
0.32 mm
0.040 mm
width = 0.400 mm
1.030 mm
B
B'
1.03 mm
0.03 mm
(a)
(b)
(c)

Figure 3

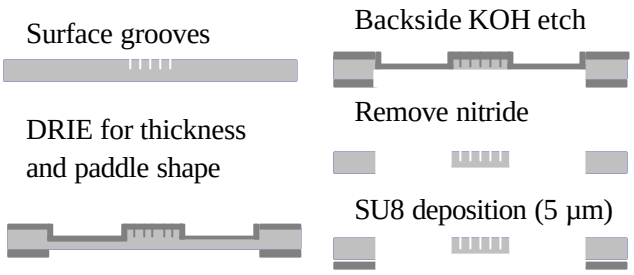
Surface grooves
Backside KOH etch
DRIE for thickness
and paddle shape
Remove nitride
SU8 deposition (5 µm)

(a)

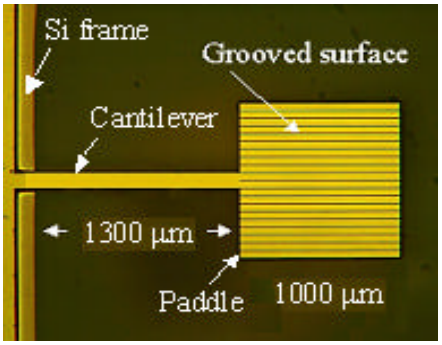
Si frame
Grooved surface
Cantilever
1300 µm
Paddle
1000 µm

(b)

Figure 4

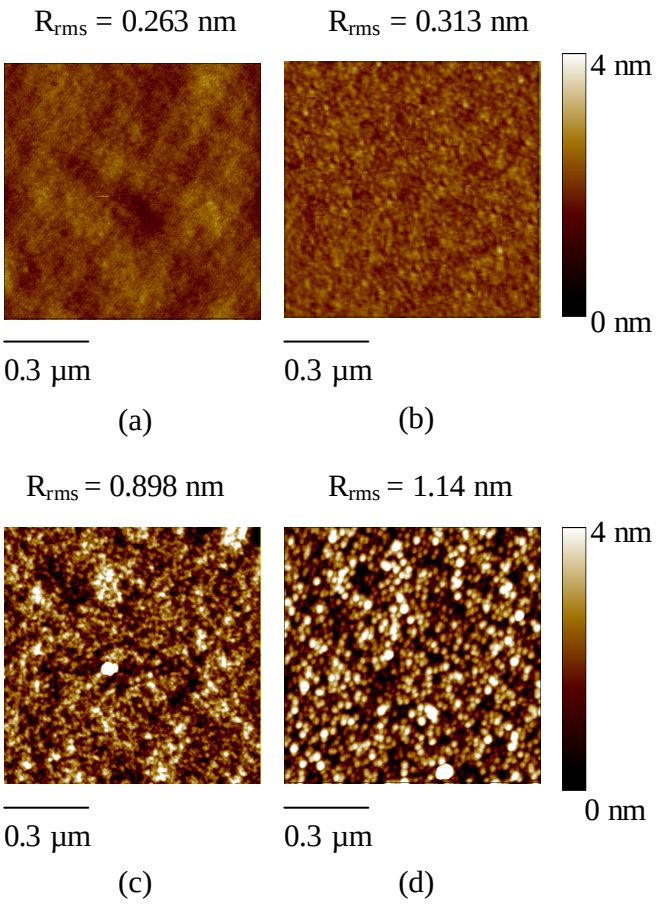
R_{rms} = 0.263 nm
R_{rms} = 0.313 nm
4 nm
0 nm
0.3 µm
0.3 µm
(a)
(b)
R_{rms} = 0.898 nm
R_{rms} = 1.14 nm
4 nm
0 nm
0.3 µm
0.3 µm
(c)
(d)

Figure 5

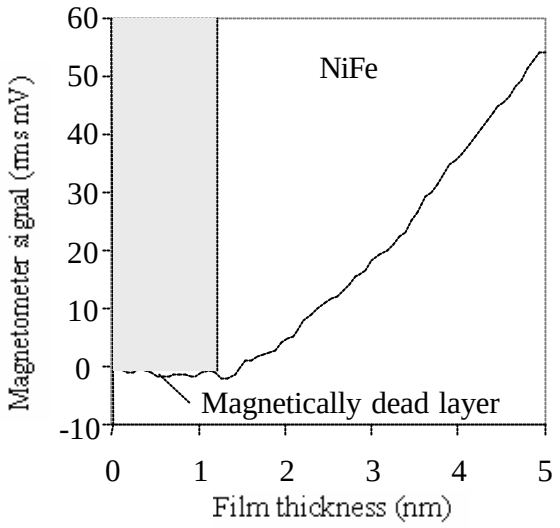
NiFe
Magnetically dead layer
Magnetometer signal (rms mV)
Film thickness (nm)
60
50
40
30
20
10
0
-10
0
1
2
3
4
5

(a)

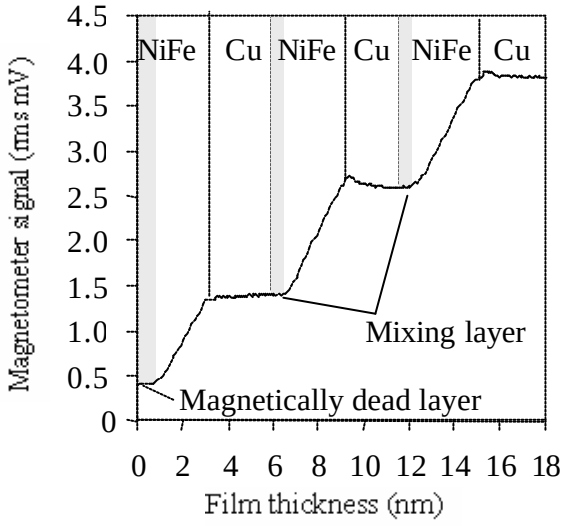
NiFe
Cu
NiFe
Cu
NiFe
Cu
Mixing layer
Magnetically dead layer
Magnetometer signal (rms mV)
Film thickness (nm)
4.5
4.0
3.5
3.0
2.5
2.0
1.5
1.0
0.5
0
0
2
4
6
8
10
12
14
16
18

(b)

Figure 6

Reference

[1] M. Löhndof, J. Moreland, and P. Kabos, Appl. Phys. Lett. **76**, (2000) pp.1176-1178.

[2] R. J. Roark, W. C. Young, Formulas for Stress and Strain, 5th Edition McGraw-Hill, (1975) 105.

[3] U. Rabe, K. Janser, and W. Arnold, Rev. Sci. Instrum. **67**, (1996) 3281.

[4] William T. Thomson, Marie Dillon Dahleh, Theory of Vibration with Applications, 5th Edition Prentice-Hall, Inc., (1998) 166.

[5] D. Sarid, Scanning Force Microscopy with Applications to Electric, Magnetic, and Atomic Forces, Oxford, New York, (1991) pp.19-38

[6] D. Rugar, H. J. Mamin, R Erlandsson, J. E. Stern, and B. D. Terris, Rev. Sci. Instrum. **59**, (1988) 2337.

[7] J.A. Sidles, J. L. Garbini, K. J. Bruland, D. Rugar, O. Zuger, S. Hoen, and C.S. Yannoni, Rev. Modern Phys. **67**, 1, (1995) pp. 249-265.

[8]] K. Lee, N. LaBianca, S. Rishton, and S. Zohlgharnain, J. Vac. Sci. Technol. B **13**, (1995) pp. 3012-3016

[9] Munir H. Nayfeh, Morton K. Brussel, Electricity and Magnetism, John Wiley and Sons, Inc., New York (1985) 352-372.

[10] Trade name is stated for technical clarity and does not imply endorsement by NIST. Products from other manufacturers may perform as well or better.

[11] P. Lu, F. Shen, S.J. O'Shea, K.H. Lee and T. Y. Ng, Mater. Phys. Mech. **4**, (2001) pp. 51-55.

[12] M. A. Ruderman and C. Kittle, Phys. Rev. **96**, (1954) 99.

[13] T. Kasuya, Prog. Theor. Phys. **16**, (1956) 45.

[14] K. Yosida, Phys. Rev. **106**, (1957) 893.